RESEARCH ARTICLE

Energy & Environmental Materials WILEY

Supercapacitors

Self-Healing All-in-One Energy Storage for Flexible Self-Powering Ammonia Smartsensors

*Hongting Ma, Fengjuan Lv, Liuxue Shen, Kaizhou Yang, Yu Jiang, Junlin Ma, Xiaodong Geng, Tongrui Sun, Yuzhen Pan, Zhuang Xie, Mianqi Xue, and Nan Zhu**

Self-healable and flexible all-in-one self-powering smartsensing devices have recently attracted great attention. Herein, a flexible all-in-one solid-state electronic system of polyvinyl alcohol (PVA) hydrogel-based supercapacitors for self-powering ammonia smartsensors has been fabricated. Self-healing supercapacitors are prepared by integrating polypyrrole (PPy) and boron cross-linked PVA/KCl hydrogel as a sandwich configuration, exhibiting large specific capacitance of 244.81 mF cm^{-2} at 0.47 mA cm^{-2}, and good charging/discharging stability of 2000 cycles, while ammonia sensors are realized by a SnO_2/PPy-modified conductive PVA hydrogel film, demonstrating an excellent sensing behavior toward NH_3 vapor under 50 ppb–500 ppm. As a result, self-healing supercapacitors could well store energy and then self-power sensing unit for remotely real-time detection via a smartphone, acquiring high flexibility of energy-sensing system. With attractive biocompatibility and self-healing performance toward various environment, this all-in-one flexible energy-smartsensor system would pave the way to novel fabrication process in realization of wearable self-healing smart devices.

1. Introduction

In recent years, there has been a growing interest in wearable electronic devices, with various practical application for healthcare monitoring,[1] motion detection,[2] or environmental analysis in high hazard surroundings.[3,4] Generally, electronic device system is composed of energy harvesting (e.g., solar energy[5]), energy storage (e.g., supercapacitors[6]), and functional utilization (e.g., fitness monitoring sensors[7]). In order to make electronic devices more biocompatible with human body,[8] researchers currently pay more attention to develop wearable and integrated electronics with stable properties after mechanical deformations.[9] Krishnamoorthy et al.[10] fabricated a self-charging supercapacitor with siloxene sheets as electrodes and siloxene-based polymeric piezofiber separator immobilized with an gel electrolyte, resulting in a perfect ability to self-charge up to a maximum of 207 mV under various levels of compressive forces. Kim et al. prepared a MoS_2 quantum sheet-based flexible symmetric supercapacitor with a high device capacitance (162 F g^{-1}).[11] Yin et al. demonstrated concept and design principles of e-textile microgrids which relied solely on human activity to work synergistically, harvesting biochemical and biomechanical energy using sweat-based biofuel cells and triboelectric generators, and regulating harvested energy via supercapacitors for high-power output.[12] These multifunctional supercapacitors with novel mechanical, surface/interfacial, thermal, electronic, photodetection, and energy harvesting/conversion functions offer attractive prospects for the design and operation of efficient, sustainable, and autonomous wearable systems.[13] However, these supercapacitors suffer from poor stretchability due to limitation of carbon cloth or textile substrates.

Owning to good performance of self-healing and high flexibility, wearable electronic devices based on hydrogels have been paid special attention. Hydrogels are tissue-like three-dimensional structures with viscoelastic, flexible, and cross-linked networks of hydrophilic polymer chain.[14,15] Electrolytic ions could be efficiently attracted and localized within hydrogel network, making solid-like hydrogels show desired liquid-like ionic conductivity.[15] Besides, moisture of quasi-solid hydrogel materials can help avoid volatilization or leakage over time.[16] Compared with original self-supporting carbon films of carbon nanotube,[17] graphene,[18] conducting polymer-based carbon films,[19] or metal oxide-based carbon films,[20] ionic conducting hydrogel exhibits higher thin-film formation ability and flexibility suffering from consecutive bending and stretching. Moreover, based on dynamic covalent bond[21–23] and noncovalent bond,[24–26] hydrogels (e.g., polyvinyl alcohol (PVA)) could build an intrinsic dynamic equilibrium of bond generation and dissociation in hydrogel networks, endowing self-healing performance. Owning to unique integration of advantageous characteristics of organic conducting materials and conventional polymers, such as hierarchically porous microstructure, inherent ionic conductivity, high mechanical flexibility, toughness, and adhesion ability,

Dr. H. Ma, F. Lv, Dr. L. Shen, K. Yang, Dr. Y. Jiang, Dr. J. Ma, X. Geng, T. Sun, Prof. Y. Pan, Prof. Z. Xie, Prof. M. Xue, Prof. N. Zhu
Zhang Dayu School of Chemistry, Dalian University of Technology, Dalian Liaoning 116024, China
E-mail: nanzhu@dlut.edu.cn
Prof. Z. Xie
School of Materials Science and Engineering and Key Laboratory for Polymeric Composite and Functional Materials of Ministry of Education, Sun Yat-sen University, Guangzhou 510275, China
Prof. M. Xue
Technical Institute of Physics and Chemistry, Chinese Academy of Sciences, Beijing 100190, China
The ORCID identification number(s) for the author(s) of this article can be found under https://doi.org/10.1002/eem2.12227.

DOI: 10.1002/eem2.12227

hydrogel is considered as a promising material for next-generation electronic devices.[27,28]

Ionic conductivity hydrogels have been widely used in wearable electronic devices over years. Xu et al. designed a self-healable supercapacitor based on a polyvinyl alcohol-borax (PVAB) hydrogel and carbon nanotube cellulose nanofiber (CNT-CNF) nanohybrids,[29] and this compact sandwich configuration (electrode-electrolyte-electrode) results into high-performance flexibility, reliability, and freedom in case of liquid leakage during measurement. Wu et al.[30] fabricated a chemically derived ionic conductive polyacrylamide/carrageenan double-network NO_2 and NH_3 sensors, withstanding various rigorous mechanical deformations (up to 1200% strain, large range flexion, and twist), and it performed high sensitivity and low theoretical limit of detection in NO_2. The previous report demonstrates that conductive hydrogels can act both as energy storage and sensor components. However, currently only a single functional application of electronic devices appears, limiting the whole flexibility and functionalization for further wearable platforms. Thus, an effective strategy is required to implement the all-in-one system for specific wearable application integrating energy storage devices with functional sensors.

Herein, a flexible all-in-one electronic system of PVA hydrogel-based supercapacitors for self-powering NH_3 sensors has been fabricated. The supercapacitor was prepared by integrating polypyrrole (PPy) and boron cross-linked PVA/KCl hydrogel as sandwich configuration (electrode-electrolyte-electrode), while NH_3 sensor was realized by a SnO_2/PPy-modified conductivity PVA hydrogel film. It is worth mentioning that supercapacitor and NH_3 sensor are designed into one system with physical cross-linking PVA hydrogel as the binder. As a result, this all-in-one device has high flexibility, good biocompatibility, and self-healing properties toward various environments. Moreover, supercapacitor stored energy from sunshine and then self-powered sensing unit for detection of analytes. Besides, wearable electronic system could be easily controlled by a cell phone for real-time monitoring. Therefore, this all-in-one self-powered integrating device has a broad prospective in practical application toward realization of advanced wearable electronics and smart energy systems.

2. Results and Discussion

2.1. Electrochemical Behaviors of Hydrogel-Based Supercapacitors

A flexible all-in-one PVA hydrogel-based system has been acquired (**Figure 1**), with supercapacitor and NH_3 sensor easily integrating into one device. Supercapacitor could store energy and then directly self-power integrated sensor without external power supply. Both supercapacitor and sensor were based on free-standing B-PVA/KCl hydrogel film. PPy was chemical oxidative polymerization on B-PVA/KCl hydrogel film for supercapacitor, while $SnO_2/FeCl_3$ solution was first dropped on film, and then PPy was coated by vapor phase polymerization for NH_3 gas sensor.

The free-standing B-PVA/KCl film was highly flexible due to physical and chemical cross-linking structure in the hydrogel (**Figure 2**a). It was reported that crystallization and phase separation of PVA during freeze-thaw physical cross-linking process could lead to gelatinization.[31] Moreover, dehydration occurred between boric acid ($B(OH)_3$) and hydroxyl groups (–OH) of PVA chains during chemical boron cross-linked process, and further improve mechanical properties of hydrogel.[31] FTIR was used to study cross-linking structure of B-PVA/KCl (Figure 2b). There appeared a peak at 650.85 cm^{-1} in B-PVA/KCl film, ascribing to O–B–O bending, which was not observed in PVA/KCl film.[32] Furthermore, the peak at 3429 cm^{-1} of –OH stretching vibration became weak after cross-linked with boric acid, indicating that boron cross-linking structure was successfully introduced into PVA molecular chains (Figure 2c).

PPy was widely used in supercapacitors because of its thermal stability, high conductivity, easy synthesis, and nontoxicity.[33] Here, PPy/B-PVA/KCl and B-PVA/KCl hydrogel films were freeze-dried for surface morphologies examined by SEM (**Figure 3**a,b), and B-PVA/KCl hydrogel film showed an interconnected porous structure, efficiently improving transmission and diffusion of molecules, ions, and electrons for obtaining high conductivity.[29] In contrast, PPy/B-PVA/KCl hydrogel film was relatively smooth with rough and orderly wavy-wrinkled structure, owning to uniform incorporation of PPy displaying on the surface of B-PVA/KCl film. It indicated that PPy could be perfectly integrated onto B-PVA/KCl film by an in situ polymerization growth method. There was a broad peak at 20.128° of XRD, revealing characteristic reflection of crystalline atactic PVA in B-PVA/KCl film (Figure 3c).[34] But this peak became sharper in PPy/B-PVA/KCl film, due to typical broad and weak reflection in the range of 15–30° of amorphous PPy.[35] Besides, other peaks in PPy/B-PVA/KCl film were obviously weak compared with B-PVA/KCl film, confirming that PPy was successfully attached into B-PVA/KCl film. The prepared flexible supercapacitor appeared to have a sandwich structure of all-in-one configuration (inset of Figure 3d) with PPy/B-PVA/KCl film as electrodes and B-PVA/KCl film as electrolyte. Due to high robust of hydrogel film, integrated supercapacitor showed excellent toughness and strength when undergoing enlarged stretching even up to 100% (Figure 3d). The excellent mechanical properties of this supercapacitor would pave great potential promising for practical application.

Capacitance performance was influenced by the concentration of pyrrole solution (0.2, 0.4, 0.6, 0.8 M) and immersion time (4, 6, 8, 10 h) (discussed in the Supporting Information). After comparison, 8-h immersion in 0.6 M pyrrole solution was chosen as optimal condition. Cyclic voltammetry (CV) and galvanostatic charge/discharge (GCD) were carried out to assess electrochemical performance of PVA hydrogel-based supercapacitors. The rectangular shapes of CV curve indicated fast charging/discharging properties of the device with high power density and predicted similar capacitive behavior with double-layer-based supercapacitors (Figure 3e).[36] In addition, areal capacitance (C_{A1}) of the supercapacitor was calculated from CV curves by using Equation (S1) as 67.6, 46.7, 37.9, 32.4, 25.8, and 21.8 mF cm^{-2} for scan rate as 25, 50, 75, 100, 150, and 200 mV s^{-1}. A substantial decrease in Cs with increase in scan rate was observed, due to decreasing number of active sites participating in the reaction during high scan rate. It is reported that, ions (K^+ and Cl^-) only reached outer surface of electrode instead of diffusing into pores of hydrogel-based electrode during high scan rate. Meanwhile, symmetrical shapes of GCD curves (Figure 3f) indicated a high reversibility of as-fabricated supercapacitor during charging/discharging processes. Areal capacitance of the supercapacitor of 244.81, 207.24, 170.82, 134, 104.52, 84.33 and 69.6 mF cm^{-2} at 0.47, 0.60, 0.73,1.00, 1.33, 1.67 and 2 mA cm^{-2}, respectively, was obtained from GCD curves by Equation (S2) (Figure 3g). The specific energy density (E) and specific power density (P) of prepared supercapacitor were calculated from GCD curves by

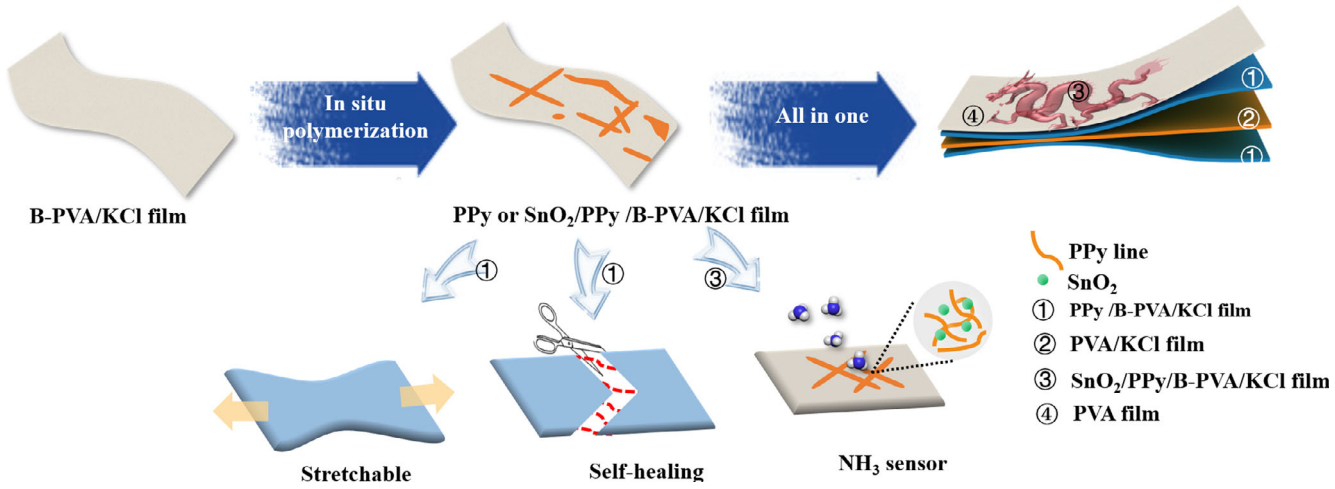

Figure 1. Schematic diagram. Preparation process for all-in-one electronic system.

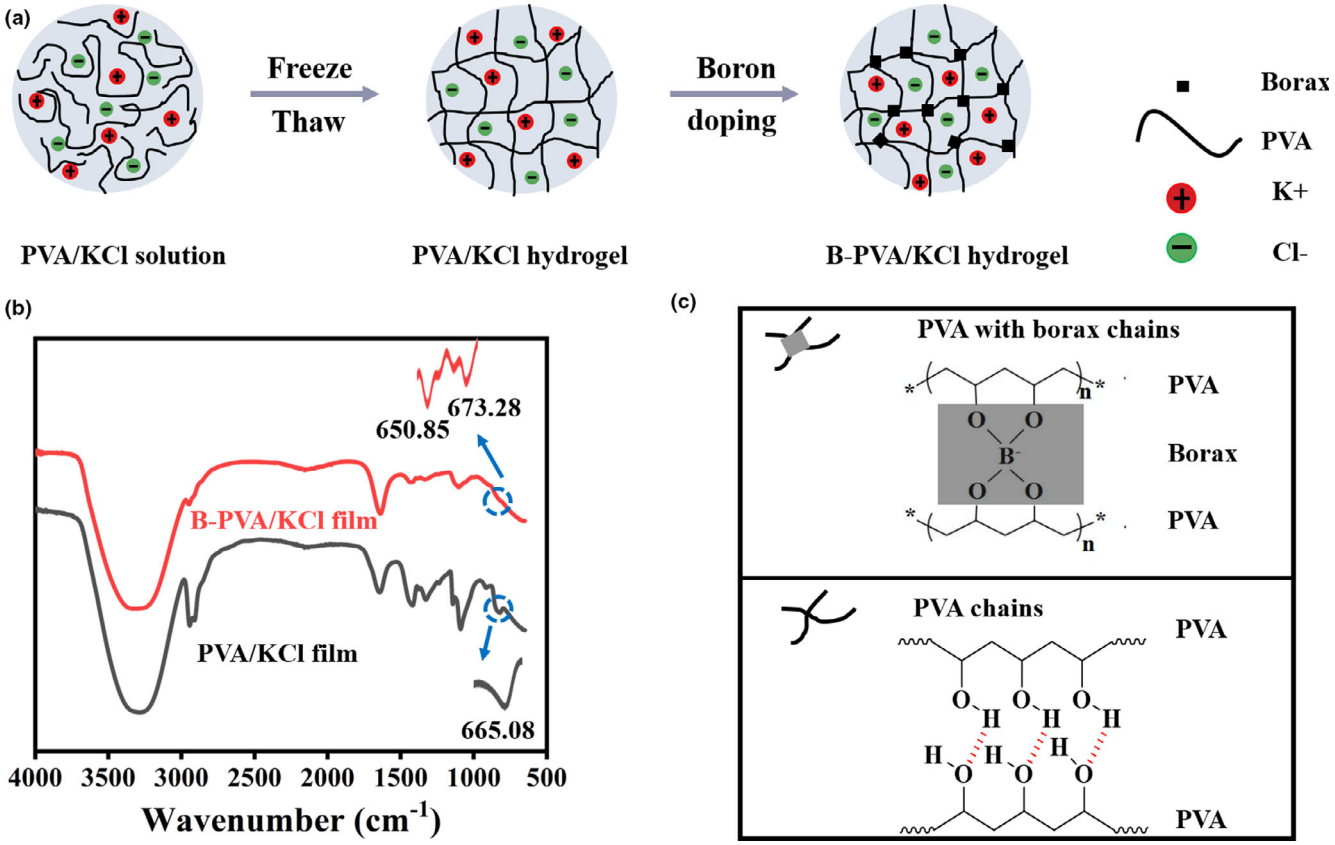

Figure 2. Characterization of in situ analysis. B-PVA/KCl hydrogel film formation mechanism. a) Schematic of cross-linking change during preparation process of B-PVA/KCl hydrogel film. b) FTIR spectra of PVA/KCl film and B-PVA/KCl film. c) The cross-linking mechanism between PVA chains and boric acid.

Equations (S3) and (S4), exhibiting a large energy density of 34.00 μWh cm^{-2} at power density of 466.67 μW cm^{-2} (Figure 3h).[37,39-42] When power density increased to 2000 μW cm^{-2}, energy density still maintained a high value of 9.67 μWh cm^{-2}. Moreover, coulombic efficiency of prepared hydrogel-based was also calculated from GCD curves as 60%, 75.21%, 75%, 77.8%, 79.12%, 80.13%, and 79.82% at current density of 0.47, 0.60, 0.73,1.00, 1.33, 1.67, and 2 mA cm^{-2}, respectively (Figure S3). The fabricated supercapacitor possessed excellent electrochemical behaviors compared with previous flexible hydrogel-based devices (Figure 3h and Table S1), attributed to effectively improving loading amount of in situ growth PPy, which was used as active material for supercapacitor.

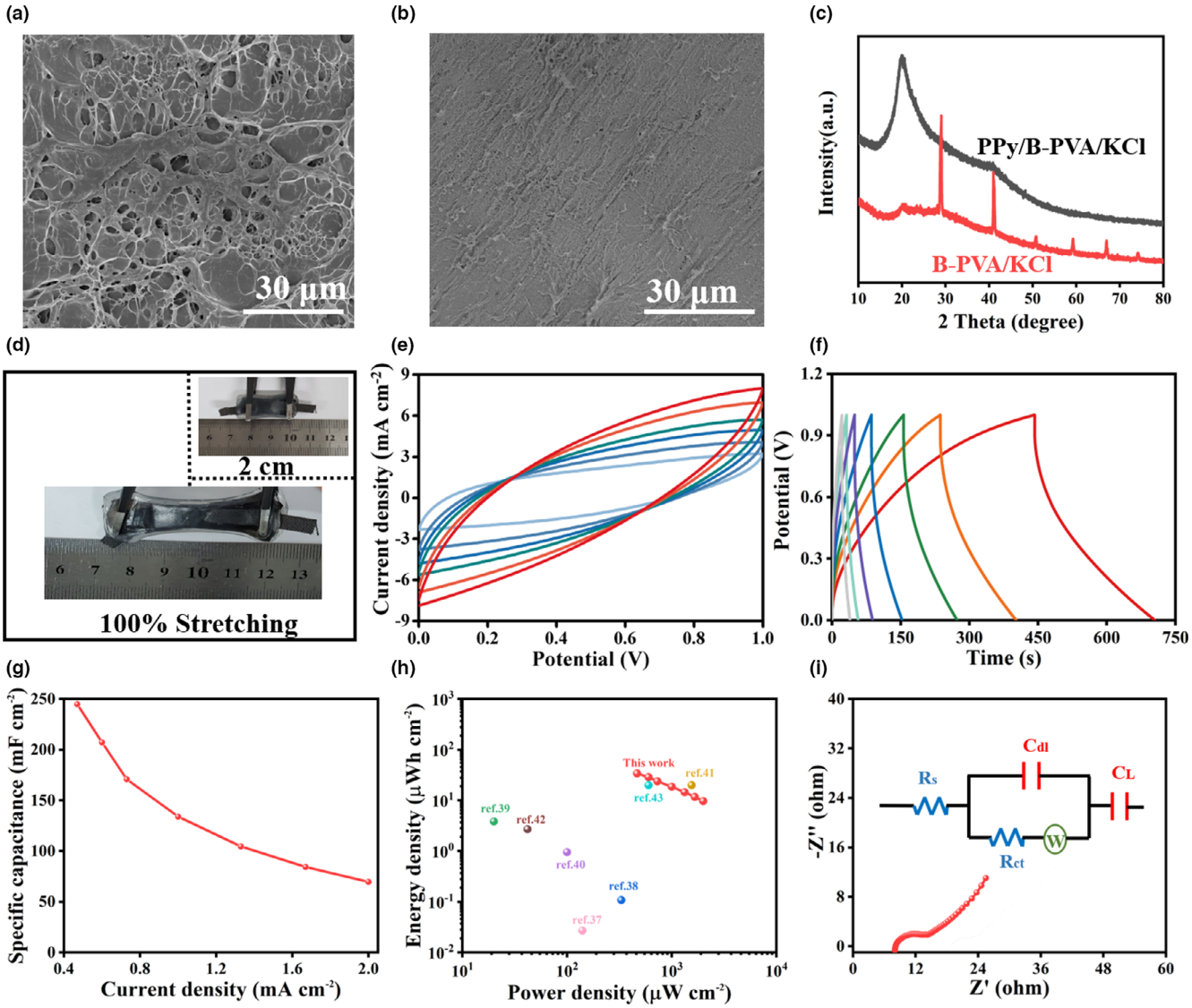

Figure 3. Characterization and electrochemical behaviors. SEM image of a) B-PVA/KCl hydrogel film and b) PPy/B-PVA/KCl hydrogel film. c) XRD patterns of B-PVA/KCl film and PPy/B-PVA/KCl film. d) Integrated supercapacitor with all-in-one configuration under 100% stretching, inset was without stretching. e) CV and f) GCD curves of supercapacitor. g) Areal capacitances of as-fabricated supercapacitor with variation of current density. h) Ragone plot. i) Nyquist impedance plots of the supercapacitor, and the inset showed an equivalent circuit fitting to Nyquist spectra.

Moreover, Nyquist impedance plots of the supercapacitor were also used to further study equivalent circuit of energy storage system. There was a small semicircle in high-frequency region and vertical line in low-frequency region in EIS spectra (Figure 3i), indicating low charge transfer resistance and good capacitive behavior with small diffusion resistance of integrated supercapacitor, respectively.[42] The electrical equivalent circuit of supercapacitor is also shown in the inset of Figure 3i, with a low series resistance (R_s) and a small interfacial charge transfer resistance (R_{ct}).[43] The suitable resistive performance of supercapacitor could be attributed to small interface contact resistance between electrode and electrolyte, as well as effective transportation of electron and ion within device.[44]

This highly flexible supercapacitor could easily power a LED, remaining bright after intense mechanical deformation of stretching and bending (**Figure 4**a). There also illustrated no obvious change from CV and GCD curves at various stretching ratios (0–50%) and bending angles (0–180°) (Figure 4b,c,e,f). Most flexible supercapacitors with multilayer laminated configuration suffered from inevitable relative displacement and even delamination between multilayers during repeated bending or stretching deformations, leading to degradation of supercapacitor performance.[34] Compared with conventional liquid electrolyte/separator configuration, this single hydrogel-based supercapacitor could overcome poor interfacial adhesion between electrode and electrolyte. As a result, capacitance retained over 90% of its initial value even after 1000 cycles of stretching/bending testing (Figure 4d,g).

Moreover, supercapacitor exhibited a superb capacitance maintaining after 2000 charge–discharge cycles (Figure 4h). It was probably attributed to slow solvent evaporation of hydrogel-based electrolyte, acquiring desired retention of ionic conductivity.[45]

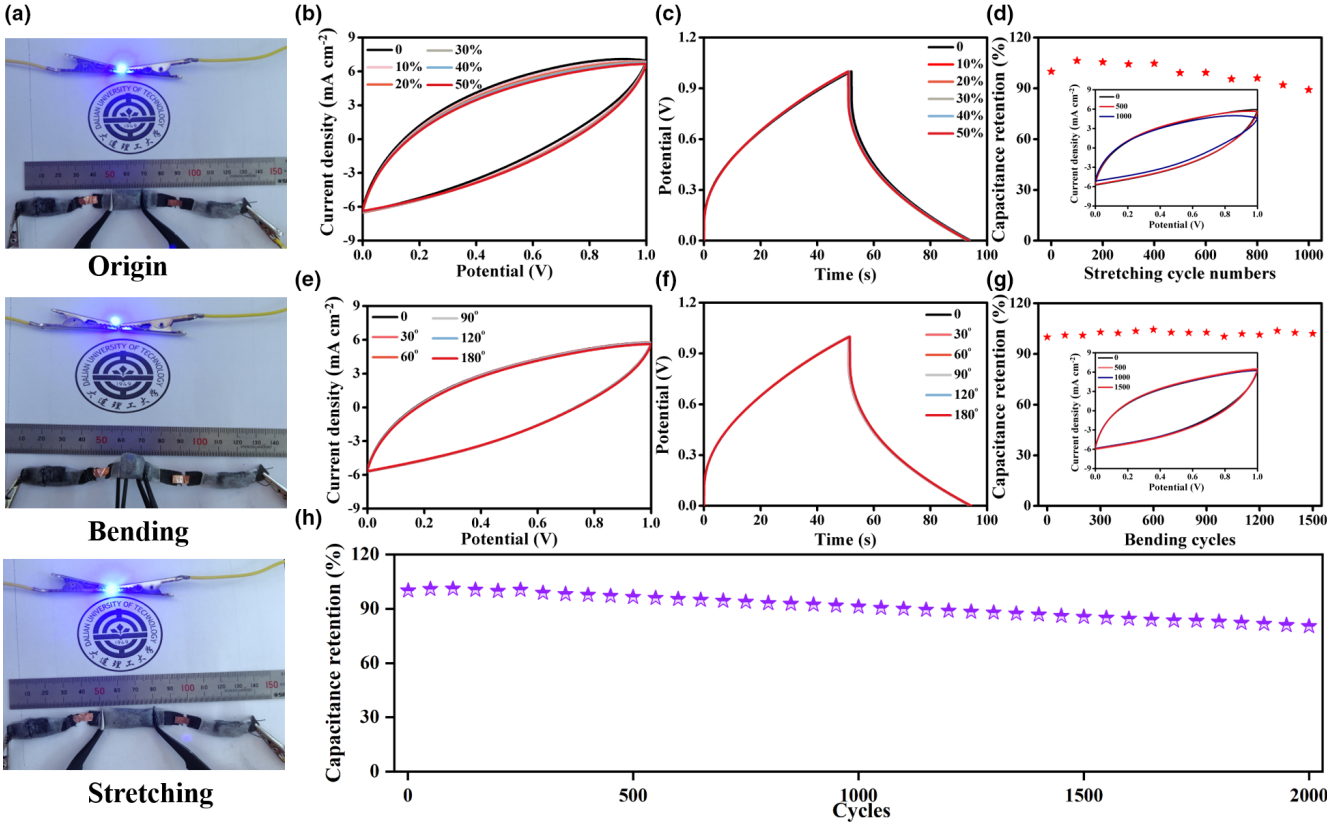

Figure 4. Bending, stretching, and cycling of supercapacitor. a) Supercapacitor for powering a LED under bending or stretching condition. Electrochemical performance of supercapacitor under different stretching ratios b) CV curves (100 mV s^{-1}) and c) GCD curves (1.33 mA cm^{-2}). d) Capacitance retention during 1000 bending–releasing cycles, and the inset showed CV curves of 0, 500, and 1000 cycles. Electrochemical performance of supercapacitor under different bending angles e) CV curves (100 mV s^{-1}) and f) GCD curves (1.33 mA cm^{-2}). g) Capacitance retention during 1000 bending–releasing cycles, and the inset showed CV curves of 0, 500, 1000, and 1500 cycles. h) Cycling performance of supercapacitor at 100 mV s^{-1}.

2.2. Self-Healing Performance of Hydrogel-Based Supercapacitors

Interestingly, this flexible supercapacitor also exhibited self-healing behavior (**Figure 5**b). Firstly, LED was powered by three series-connected supercapacitors. Secondly, LED closed after one supercapacitor was cut off. After that, two broken pieces were tightly aligned and heated to 85 °C for 20 s, surfaces could tightly adhere to each other and then light turned bright again. More importantly, there was negligible change in the brightness of self-healed device under stretching or bending deformation, suggesting outstanding self-healable property of physical and chemical cross-linking B-PVA/KCl hydrogel film. More specific self-healing performance was demonstrated in Figure 5c,d. Capacitance recovered as regular after self-healing process, and even stable during bending of various angles (30°, 60°, 90°).[46] Thus, the supercapacitor could maintain its original mechanical strength and charge transport capability after self-healing process. Such self-healing capability could greatly prolong lifetime of supercapacitors, providing a novel platform for designing a new-generation flexible electronic device.

Self-healable mechanism results from physical and chemical boron cross-linking process in B-PVA/KCl hydrogel film. Firstly, tetrahedron-shaped $[B(OH)_4]^-$ dissociated from boric acid could reversibly coordinate with free –OH groups,[47] contributing to rapid self-healing capability of hydrogels without healing agents or external stimuli (Figure 5a).[48] Secondly, reformation of cross-linked network was accomplished by diffusion of PVA chains across surface of disconnection with physical entanglements of polymer chains, and their subsequent interchain hydrogen bond interactions.[49] Heating process promoted ion dissociation of intra- or intermolecular in PVA hydrogel and dynamical cross-links created by reversible hydrogen bonds, which was a crucial role in quick and efficient self-healing performance of hydrogel film. Physical and chemical cross-linking endowed hydrogel film with good mechanical performance, avoiding delamination or dislocation of interfaces between electrolyte and electrode, and remaining original structure for electrochemical performance after self-healing (details in the Supporting Information).

2.3. Sensing Performance of NH_3 Sensors

Additionally, this all-in-one supercapacitor of SnO_2/PPy-B-PVA/KCl hydrogel could be used as a sensing device for gas detection (**Figure 6**). The morphologies and microstructures of prepared SnO_2 and SnO_2/PPy hybrid were studied by SEM (Figure S5a,b), XRD (Figure S5c), and FTIR (Figure S5d) and discussed in the Supporting Information. An excellent sensing behavior was observed toward NH_3 gas under 50 ppb–500 ppm of 50% RH (**Figure 6**a), where response

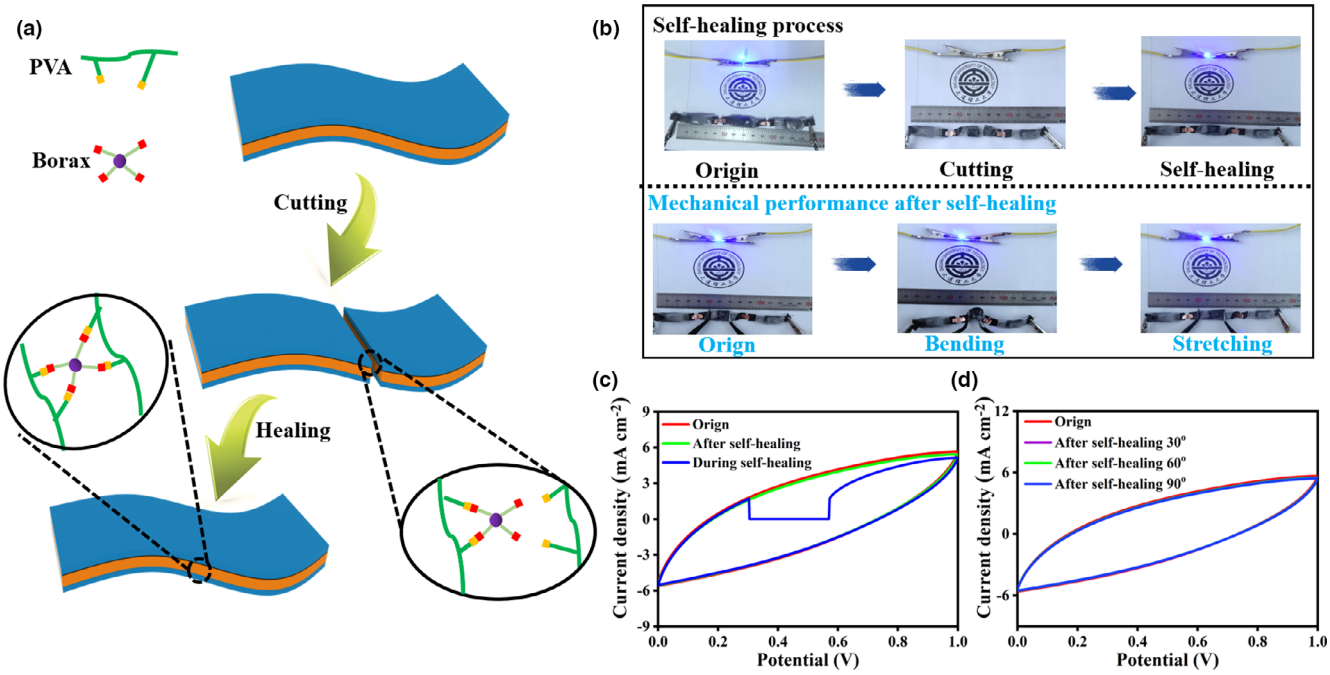

Figure 5. Self-healing performance of the supercapacitor. a) Schematic illustration of self-healable mechanism of supercapacitor.[25] b) Three series-connected supercapacitors during self-healing process. c) CV performance during self-healing process. d) CV curves of healed supercapacitor under different bending angles.

($\Delta R/R_0$) increased upon ammonia, and the fitting curves of sensor to different concentrations of NH_3 are shown in Figure S6a,b.[50-52] Low detection limit of ammonia (1.573% at 50 ppb) would result from good combination between PPy and SnO_2 nanoparticles on B-PVA/KCl film, leaving abundant amount of reaction sites on sensing surface.[52] Furthermore, good repeatable characteristic was also illustrated toward same concentration of 50 ppb NH_3 (Figure 6a inset). Response and recovery time of ammonia (50 ppb) were 124 and 68 s, respectively (Figure 6a inset), indicating a fast-sensing reaction for analytes. As a result, this hydrogel sensor demonstrated better sensing performance compared with existing reports (Table S2).

Sensing mechanism of NH_3 came from synergic effect of p-n junction with p-type PPy and n-type SnO_2.[53] The reaction process of NH_3 sensor for p-type PPy is shown in Equation (1). When the sensor was exposed to NH_3 gas, electron/proton transfer occurs, leading to charge compensation.[54-58]

For n-type SnO_2, the reaction process can be simplified as given in the following Equations (2)–(4). Oxygen would firstly react with metal oxide and then form oxygen ions (O^{2-}, O^-, O_2^-) (Equation 2).[59,60]

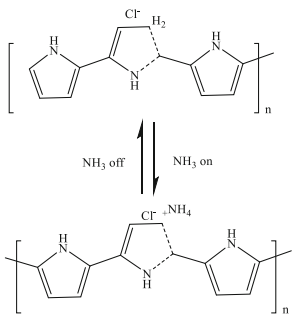

(1)

Owning to greater electronegativity of oxygen molecules, electrons would escape from conduction band of SnO_2, leading to decrease in the concentration of free charge carriers. As a result, a depletion layer (LD) at grain boundaries would be received. Once NH_3 gas was introduced into the surface of sensor, oxygen species interact with NH_3, resulting in the formation of NO_X (Equations 3 and 4). Meanwhile, free electrons will return to conduction band of SnO_2, greatly compressing LD and increasing the resistance of metal oxides.

$$O_2 + 2e^- \xrightarrow{SnO_2} \begin{cases} O_2^- \\ 2O^- \end{cases} \quad (2)$$

$$4NH_3 + 5O_2^- \rightarrow 4NO + 6H_2O + 5e^- \quad (3)$$

$$2NH_3 + 3O^- \rightarrow N_2 + 3H_2O + 3e^- \quad (4)$$

When p-type semiconductors PPy contact with n-type SnO_2, holes near p-n junction in p-type PPy will diffuse into n-type SnO_2, neutralizing free electrons and forming a new region C (Figure 6b). Meanwhile, free electrons in SnO_2 will also diffuse into PPy, neutralizing the holes and forming another new region B. Thus, a p-n junction of space charge region (LD) will form between p-type PPy and n-type SnO_2 (details in the Supporting Information),[61] and the whole SnO_2/PPy nanostructure could be divided into 4 regions (region A, B, C and D) (Figure 6b).

Additionally, *I-V* curves toward different vapor polymerization times of 10–180 min were measured to further prove the formation of p-n junction (Figure S8a). The resistance of this device increased with polymerization time increasing within 30 min, but decreased over 30 min, which was consistent with the report.[62] Briefly, the overall resistance (*R*) could be represented as Equation (5),

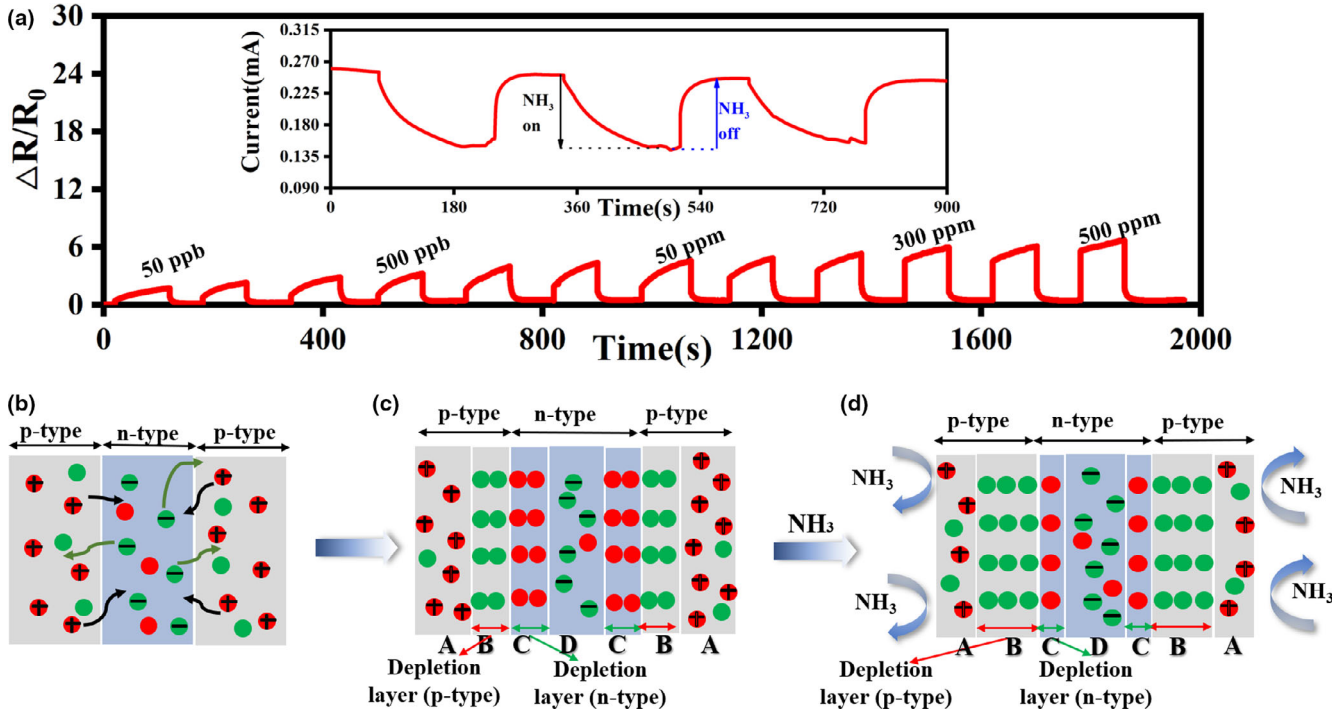

Figure 6. Electrochemical performance of the NH_3 sensor. a) Dynamical response to various concentrations (0.05, 0.1, 0.25, 0.5, 5, 10, 50, 100, 200, 300, 400, 500 ppm) of NH_3 at room temperature, and inset showed reversibility of sensor under 50 ppb NH_3 condition. b,c,d) Schematic diagram of SnO_2/PPy-B-PVA/KCl hydrogel film sensing mechanism for NH_3 sensor.

$$\frac{1}{R}=\frac{1}{R_A}+\frac{1}{R_B}+\frac{1}{R_C}+\frac{1}{R_D} \quad (5)$$

where R_A, R_B, R_C, and R_D are the resistance of four regions A, B, C and D, respectively. Considering the value of R_C or R_D for SnO_2 to be much larger than R_A or R_B for PPy, the overall resistance (R) can be simplified as Equation (6),

$$\frac{1}{R}=\frac{1}{R_A}+\frac{1}{R_B} \quad (6)$$

When polymerization time was less than 30 min, the thickness of region A was thinner than that of region B. PPy layer will increase with polymerization time, and more holes from PPy will enter into SnO_2 for neutralizing free electrons, resulting in improved resistance. While polymerization time was over 30 min, region A was much thicker than region B, and hole transfer could be negligible compared with high conductivity of PPy layer. So the resistance will decrease toward increasing polymerized PPy layer under this circumstance.

Moreover, dynamical response to 50 ppb NH_3 at room temperature with different vapor polymerization times (5, 10, 15, 20, 25, 30, 60, 120, and 180 min) has been detected (Figure S8b), and the sensor showed maximum response with polymerization of 60 min. When the sensor was exposed to NH_3, holes from region A and B will both react with NH_3, leading to the decrease in holes for enlarging R_A and R_B.[51,52,62] At the same time, holes from region C will move to region B in equilibrium, making thickness of region C to reduce and region B to increase (Figure 6b,c). The thickness of region A and B was also critical keys to response signals. When the thickness of region A was thinner or equal to that of region B (polymerization time of 5–30 min), R was dependent on R_B. The variation of residual holes from region B will increase with increase in polymerized PPy layer, resulting in a larger response. While region A was thicker than region B (polymerization time over 30 min), R_A and R_B both contributed to R, and the response to NH_3 mainly depend on the thickness of region A. As a result, the response would decrease with increase in the thickness of region A, due to low diffusion rate toward NH_3 within inner sensing body.[51]

Besides, several volatile of solvents (VOCs), which commonly exist with ammonia in the environment of laboratory, workshop, chemical plant, or experimental samples, were chosen to study the selectivity properties of this sensor (Figure S9). At first, the resistance of sensor increased obviously after introduction of 50 ppb NH_3 gas, while negligibly changed when other six types of VOCs (50 ppb) were introduced. Besides, the resistance increased with further addition of 50 ppb NH_3, indicating high selective behavior of PPy/SnO_2-modified B-PVA/KCl-based sensor for ammonia detection with compared to other analytes. The selective performance of this sensor may be explained on basis of sensing mechanism. During sensing process, total conduction mostly relied on intra-chain's contribution rather than interchain.[63] Moreover, it is reported that polypyrrole was de-doped under the ammonia presence, affecting intra-chain conduction in polypyrrole.[64] Therefore, the response of SnO_2/PPy-based sensor was expected to be substantially higher for ammonia detection compared with other analytes, achieving accurate detection of ammonia vapor among these VOCs without interference.

2.4. Integrated Electronic Supercapacitors for Self-Powering NH_3 Sensing

To further evaluate practical application of this all-in-one hydrogel self-powered sensor system, supercapacitor and NH_3 sensor were integrated

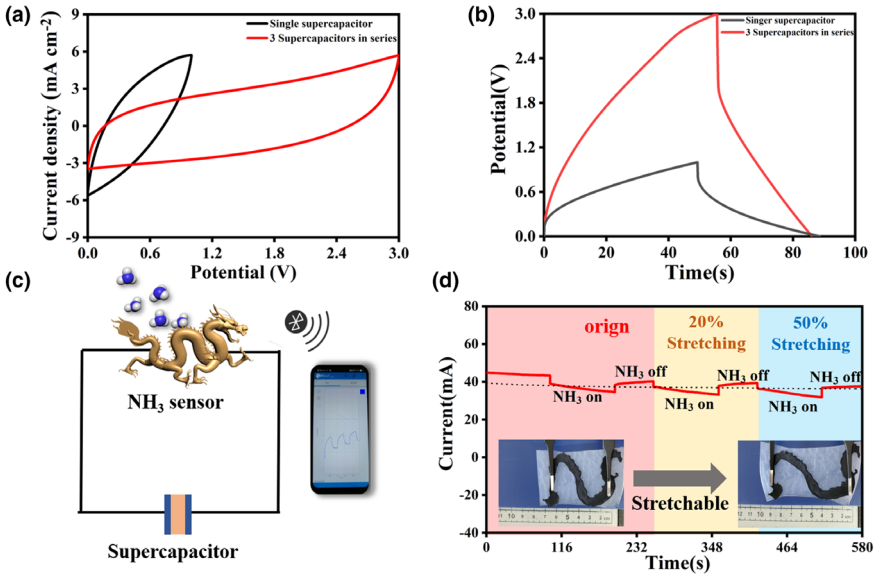

Figure 7. Electrochemical performance of the integrated electronic system. a) CV and b) GCD curves for comparison of three supercapacitors connected in series (red plot) and single supercapacitors (black plot). c) Equivalent circuit of integrated electronic system for wireless monitoring of NH_3. d) Dynamical response of sensor under 50 ppb NH_3 at room temperature during stretching process (0%, 20%, and 50%).

into one device with 20 wt.% PVA solution as binder and the equivalent circuit diagram is shown in **Figure 7**c. NH_3 sensor could be powered by prepared supercapacitor. A dragon shape of integrated device was designed to enhance stretchable performance. Briefly, supercapacitor was first fully charged by a commercial solar cell, and then it powered ammonia sensor for remotely real-time detection via a cell phone. Output voltage could increase to 3 V by connecting three supercapacitors in series (Figure 7a,b) and provide a stable voltage after 900 s for self-powered sensing measurement (Figure S10, black line). As a result, during self-powered sensing process, it could be considered that current only changed with ammonia vapor on/off (Figure 7d, red line).

Self-powered NH_3 sensor performance of $\Delta R/R_0 \approx 1.4$ was in accordance with NH_3 concentration (50 ppb) during 0%, 20%, and 50% stretching process (Figure 7d), which was similar to the response in direct sensing testing of $\Delta R/R_0 \approx 1.5$ (Figure 6a).

The stability of all-in-one electronic system was also studied and the device could stay for one week by inter-day and intra-day testing in an ideal range (Figure S11). Thus, this flexible all-in-one system would offer a self-powered sensing behavior for further practical application. As reported, PVA hydrogels have been widely used in tissue engineering,[65] drug delivery,[66] energy storage devices,[67] etc., because of their resemblance to biological tissues and nontoxicity. Meanwhile, active materials of supercapacitor (PPy) were also reported to be used in efficient biomimetic systems, such as artificial muscles[68] or drug delivery,[69] with bio-conformability and capability to electronically control a wide range of physical and chemical properties. Thanks to biocompatible properties of our system, skin allergy test of all-in-one electric system in the hands of volunteer during NH_3 sensing process has been further studied. As shown in Figure S12, electronic device was simply taped to t tester's wrist, and NH_3 vapor was brought out by a constant nitrogen flow from aqueous solution, containing certain concentration of ammonia. It is obviously that there were no allergies observed during hours of charging/discharging and sensing process, indicating safety nontoxicity and potential of the device to be used in wearable electronic field.

3. Conclusion

In this work, a flexible hydrogel-based all-in-one electronic system consisting of supercapacitors and NH_3 sensors has been fabricated. This all-in-one solid-state device has high flexibility, good biocompatibility, stretchable and self-healing properties toward various environment. Supercapacitors were prepared by integrating PPy and boron cross-linked PVA/KCl hydrogel as sandwich configuration (electrode-electrolyte-electrode), while NH_3 sensor was realized by a SnO_2/PPy-modified conductivity PVA hydrogel film. Supercapacitors and NH_3 sensors were integrated via physical cross-linking PVA hydrogel as binder. As a result, supercapacitor could store energy and then self-power NH_3 sensing unit. Besides, wearable electronic system could also wirelessly control real-time monitor NH_3 gas sensor by a cellphone. This all-in-one system demonstrates a novel fabricated process and practical application of highly flexible supercapacitors to self-power integrated sensors in advanced wearable electronics and smart energy devices. In future study, additional functional devices, such as voltage stabilizer, will be integrated into all-in-one system, to acquire a stable output voltage for wearable practical applications.

4. Experimental Section

Preparation of boron cross-linked PVA/KCl hydrogel film (B-PVA/KCl): The free-standing B-PVA/KCl film consisted both physical and chemical cross-link, with mechanism shown in Figure 2a.[44] 10 mL 10wt. % transparent PVA gel solution was under stirring at 85 °C for 2 h. Then, 3 mL KCl solution (3 M) was added into the above solution with 30-min constant stirring. After that, the mixture was poured into plastic mold (1 × 1.5 × 0.1 cm^3), frozen at −15 °C for 24 h, and thawed at room temperature for 12 h. After three freeze-thaw cycles, free-standing PVA/KCl hydrogel film was peeled off from the mold and immersed in boric acid/ammonia solution (1 mg mL^{-1}, pH = 11) for 24 h, acquiring chemical cross-link between PVA chains and boric acid.

Preparation of PPy/B-PVA/KCl hydrogel film: The PPy/B-PVA/KCl hydrogel film was prepared through chemical oxidative polymerization process. Firstly, as-prepared B-PVA/KCl hydrogel film was immersed in pyrrole solution with dissolved APS (pyrrole/APS molar ratio = 1:2) at 4 °C for several hours to allow complete polymerization of pyrrole. Then, hydrogel film was taken out and washed several times with deionized water. The concentration of pyrrole solution was 0.2, 0.4, 0.6, and 0.8 M and immersing time was 4, 6, 8, and 10 h, respectively, for measuring the performance of supercapacitors.

Fabrication of all-in-one flexible supercapacitors: Firstly, a piece of B-PVA/KCl electrolyte layer (1.2 × 1.8 × 0.3 cm^3) was placed between two pieces of free-standing PPy/B-PVA/KCl electrode layers (1 × 1.5 × 0.1 cm^3). Secondly, two identical carbon cloth strips were tightly affixed to both sides as the collector. Finally, two pieces of nonconducting PVA films (detail process in the Supporting Information) were used to encapsulate the device under a pressure of ~0.5 MPa, with 20 wt.% PVA solution as the adhesion agent.

Fabrication of NH_3 gas sensor: The SnO_2/PPy-modified B-PVA/KCl layer was prepared by vapor phase polymerization of pyrrole.[70] Firstly, 0.1 g of anhydrous $FeCl_3$ was dissolved in 5 mL deionized water. Then, SnO_2 samples (detail synthesis

process in the Supporting Information) were dipped into the solution and stirred for 30 min. Then yellow suspension was dropped on B-PVA/KCl hydrogel film and left dried in open air for 1 h. Finally, prepared film was further exposed to pyrrole (Py) monomers in a closed chamber for 1 h. During sensing process of ammonia sensor, NH_3 vapor was brought out by a constant nitrogen flow from its aqueous solution, which contains certain concentration ammonia. The vapor was drained from rubber conduit to sensing electrode surface and maintained 1 min before each test to ensure test environment is stable. Meanwhile, gas flow rate was controlled by gas flow meter.

Electrochemical measurements: Cyclic voltammetry (CV) and galvanostatic charge/discharge (GCD) of the supercapacitor were measured by CHI 600E (Shanghai Chenhua instrument Co., Ltd., China). CV was tested at different scan rates of 25, 50, 100, 150, 200 and 250 mV s^{-1}. GCD was measured at 0.47, 0.6, 0.73, 1, 1.33, 1.67 and 2 mA cm^{-2} current density. Calculations of areal capacitance or specific power can be found in the Supporting Information. The testing of NH_3 gas sensor was carried out in a gas chamber. Two electrodes were applied a constant bias voltage of 0.5 V by amperometric (i-t). Detailed measurements can be found in Supporting Information. The sensor was powered by three series-connected supercapacitors with a stable output voltage of about 0.5 V.

Acknowledgements

We are grateful for the financial support from National Natural Science Foundation of China (Grant No. 22074010), Dalian Science and Technology Bureau, China (Grant No. 2019J12SN54), Basic and Applied Basic Research Program of Guangzhou City, China (Grant No. 202002030434), and Zhang Dayu School of Chemistry, Dalian University of Technology, China.

Conflict of Interest

The authors declare no conflict of interest.

Supporting Information

Supporting Information is available from the Wiley Online Library or from the author.

Keywords

ammonia sensor, flexible supercapacitor, hydrogel, self-healing, self-power

Received: February 20, 2021
Revised: May 3, 2021
Published online: May 25, 2021

[1] S. Imani, A. J. Bandodkar, A. M. Mohan, R. Kumar, S. Yu, J. Wang, P. P. Mercier, *Nat. Commun.* **2016**, *7*, 11650.
[2] T. Q. Trung, N. E. Lee, *Adv. Mater.* **2016**, *28*, 4338.
[3] R. K. Mishra, A. Martín, T. Nakagawa, A. Barfidokht, X. Lu, J. R. Sempionatto, K. M. Lyu, A. Karajic, M. M. Musameh, I. L. Kyratzis, J. Wang, *Biosens. Bioelectron.* **2018**, *101*, 227.
[4] A. Barfidokht, R. K. Mishra, R. Seenivasan, S. Liu, L. J. Hubble, J. Wang, D. A. Hall, *Sens. Actuators B Chem.* **2019**, *296*, 126422.
[5] S. Xie, R. Xia, Z. Chen, J. Tian, L. Yan, M. Ren, Z. Li, G. Zhang, Q. Xue, H.-L. Yip, Y. Cao, *Nano Energy* **2020**, *78*, 105238.
[6] V. Rajendran, A. M. V. Mohan, M. Jayaraman, T. Nakagawa, *Nano Energy* **2019**, *65*, 104055.
[7] H. Ma, Y. Jiang, J. Ma, X. Ma, M. Xue, N. Zhu, *Anal. Chem.* **2020**, *92*, 5897.
[8] M. F. El-Kady, R. B. Kaner, *Nat. Commun.* **2013**, *4*, 1475.
[9] Q. C. Liu, J. J. Xu, D. Xu, X. B. Zhang, *Nat. Commun.* **2015**, *6*, 7892.
[10] K. Krishnamoorthy, P. Pazhamalai, V. K. Mariappan, S. S. Nardekar, S. Sahoo, S. J. Kim, *Nat. Commun.* **2020**, *11*, 2351.
[11] S. S. Nardekar, K. Krishnamoorthy, P. Pazhamalai, S. Sahoo, V. K. Mariappan, S.-J. Kim, *J. Mater. Chem. A* **2020**, *8*, 13121.
[12] L. Yin, K. N. Kim, J. Lv, F. Tehrani, M. Lin, Z. Lin, J. M. Moon, J. Ma, J. Yu, S. Xu, J. Wang, *Nat. Commun.* **2021**, *12*, 1542.
[13] Y. Zhou, H. Qi, J. Yang, Z. Bo, F. Huang, M. S. Islam, X. Lu, L. Dai, R. Amal, C. H. Wang, Z. Han, *Energy Environ. Sci.* **2021**, *14*, 1854.
[14] Q. Wang, J. L. Mynar, M. Yoshida, E. Lee, M. Lee, K. Okuro, K. Kinbara, T. Aida, *Nature* **2010**, *463*, 339.
[15] C. C. Kim, H. H. Lee, K. H. Oh, J. Y. Sun, *Science* **2016**, *353*, 682.
[16] M. Jiang, J. Zhu, C. Chen, Y. Lu, Y. Ge, X. Zhang, *ACS Appl. Mater. Interfaces* **2016**, *8*, 3473.
[17] P. Wu, S. Cheng, M. Yao, L. Yang, Y. Zhu, P. Liu, O. Xing, J. Zhou, M. Wang, H. Luo, M. Liu, *Adv. Func. Mater.* **2017**, *27*, 1702160.
[18] L. Huang, D. Santiago, P. Loyselle, L. Dai, *Small* **2018**, *14*, e1800879.
[19] C. Meng, C. Liu, L. Chen, C. Hu, S. Fan, *Nano Lett.* **2010**, *10*, 4025.
[20] L. Huang, D. Chen, Y. Ding, S. Feng, Z. L. Wang, M. Liu, *Nano Lett.* **2013**, *13*, 3135.
[21] J. M. Lehn, *Chem. Soc. Rev.* **2007**, *36*, 151.
[22] J.-M. Lehn, *Prog. Polym. Sci.* **2005**, *30*, 814.
[23] T. Maeda, H. Otsuka, A. Takahara, *Prog. Polym. Sci.* **2009**, *34*, 581.
[24] J. Cui, A. del Campo, *Chem. Commun. (Camb)* **2012**, *48*, 9302.
[25] T. Kakuta, Y. Takashima, M. Nakahata, M. Otsubo, H. Yamaguchi, A. Harada, *Adv. Mater.* **2013**, *25*, 2849.
[26] M. Nakahata, Y. Takashima, H. Yamaguchi, A. Harada, *Nat. Commun.* **2011**, *2*, 511.
[27] Y. Shi, L. Pan, B. Liu, Y. Wang, Y. Cui, Z. Bao, G. Yu, *J. Mater. Chem. A* **2014**, *2*, 6086.
[28] Y. Shi, L. Peng, G. Yu, *Nanoscale* **2015**, *7*, 12796.
[29] J. Han, H. Wang, Y. Yue, C. Mei, J. Chen, C. Huang, Q. Wu, X. Xu, *Carbon* **2019**, *149*, 1.
[30] J. Wu, Z. Wu, S. Han, B. R. Yang, X. Gui, K. Tao, C. Liu, J. Miao, L. K. Norford, *ACS Appl. Mater. Interfaces* **2019**, *11*, 2364.
[31] J. L. Holloway, A. M. Lowman, G. R. Palmese, *Soft Matter* **2013**, *9*, 826.
[32] Y.-F. Huang, P.-F. Wu, M.-Q. Zhang, W.-H. Ruan, E. P. Giannelis, *Electrochim. Acta* **2014**, *132*, 103.
[33] C. Li, H. Bai, G. Shi, *Chem. Soc. Rev.* **2009**, *38*, 2397.
[34] K. Wang, X. Zhang, C. Li, X. Sun, Q. Meng, Y. Ma, Z. Wei, *Adv. Mater.* **2015**, *27*, 7451.
[35] G. Ma, H. Peng, J. Mu, H. Huang, X. Zhou, Z. Lei, *J. Power Sources* **2013**, *229*, 72.
[36] T. Chen, R. Hao, H. Peng, L. Dai, *Angew. Chem. Int. Ed. Engl.* **2015**, *54*, 618.
[37] J. Bae, M. K. Song, Y. J. Park, J. M. Kim, M. Liu, Z. L. Wang, *Angew. Chem. Int. Ed. Engl.* **2011**, *50*, 1683.
[38] L. Kou, T. Huang, B. Zheng, Y. Han, X. Zhao, K. Gopalsamy, H. Sun, C. Gao, *Nat. Commun.* **2014**, *5*, 3754.
[39] Y. Fu, H. Wu, S. Ye, X. Cai, X. Yu, S. Hou, H. Kafafy, D. Zou, *Energy Environ. Sci.* **2013**, *6*, 805.
[40] K. Gao, Z. Shao, J. Li, X. Wang, X. Peng, W. Wang, F. Wang, *J. Mater. Chem. A* **2013**, *1*, 63.
[41] Y. Fu, X. Cai, H. Wu, Z. Lv, S. Hou, M. Peng, X. Yu, D. Zou, *Adv. Mater.* **2012**, *24*, 5713.
[42] J.-G. Wang, Y. Yang, Z.-H. Huang, F. Kang, *Carbon* **2013**, *61*, 190.
[43] J. Wang, Y. Xu, F. Yan, J. Zhu, J. Wang, *J. Power Sources* **2011**, *196*, 2373.
[44] K. Sun, E. Feng, G. Zhao, H. Peng, G. Wei, Y. Lv, G. Ma, *ACS Sustain. Chem. Eng.* **2018**, *7*, 165.
[45] Y. Jin, H. Chen, M. Chen, N. Liu, Q. Li, *ACS Appl. Mater. Interfaces* **2013**, *5*, 3408.
[46] Y. Huang, M. Zhong, Y. Huang, M. Zhu, Z. Pei, Z. Wang, Q. Xue, X. Xie, C. Zhi, *Nat. Commun.* **2015**, *6*, 10310.

[47] W. P. Chen, D. Z. Hao, W. J. Hao, X. L. Guo, L. Jiang, *ACS Appl. Mater. Interfaces* **2018**, *10*, 1258.
[48] S. Spoljaric, A. Salminen, N. D. Luong, J. Seppälä, *Eur. Polymer J.* **2014**, *56*, 105.
[49] H. Zhang, H. Xia, Y. Zhao, *ACS Macro. Lett.* **2012**, *1*, 1233.
[50] Y. Li, H. Ban, M. Yang, *Sens. Actuators B Chem.* **2016**, *224*, 449.
[51] T. Jiang, Z. Wang, Z. Li, W. Wang, X. Xu, X. Liu, J. Wang, C. Wang, *J. Mater. Chem. C* **2013**, *1*, 3017.
[52] A. Beniwal, P. K. Sahu, S. Sharma, *J. Sol-Gel. Sci. Technol.* **2018**, *88*, 322.
[53] J. Ren, W. Bai, G. Guan, Y. Zhang, H. Peng, *Adv. Mater.* **2013**, *25*, 5965.
[54] M. Sofos, J. Goldberger, D. A. Stone, J. E. Allen, Q. Ma, D. J. Herman, W. W. Tsai, L. J. Lauhon, S. I. Stupp, *Nat. Mater.* **2009**, *8*, 68.
[55] S. Möller, S. R. Forrest, C. Perlov, W. Jackson, C. Taussig, *J. Appl. Phys.* **2003**, *94*, 7811.
[56] J. K. Haiqing Liu, D. A. Czaplewski, H. G. Craighead, *Nano Lett.* **2004**, *4*, 671.
[57] F. Yakuphanoglu, *Synth. Met.* **2007**, *157*, 859.
[58] B. K. Sharma, N. Khare, S. Ahmad, *Solid State Commun.* **2009**, *149*, 771.
[59] C. S. Rout, M. Hegde, A. Govindaraj, C. N. R. Rao, *Nanotechnology* **2007**, *18*, 205504.
[60] K. Khun Khun, A. Mahajan, R. K. Bedi, *J. Appl. Phys.* **2009**, *106*, 124509.
[61] A. Kaur, R. Kumar, *Sens. Actuators A Phys.* **2016**, *245*, 113.
[62] S. Bagchi, R. Achla, S. K. Mondal, *Sens. Actuators B Chem.* **2017**, *250*, 52.
[63] M. Joulazadeh, A. H. Navarchian, *Synth. Met.* **2015**, *210*, 404.
[64] A. Beniwal, Sunny, *Sens. Actuators B Chem.* **2019**, *296*.
[65] K. Y. Lee, D. J. Mooney, *Chem. Rev.* **2001**, *101*, 1869.
[66] J. Li, D. J. Mooney, *Nat. Rev. Mater.* **2016**, *1*.
[67] Y. Huang, M. Zhong, F. Shi, X. Liu, Z. Tang, Y. Wang, Y. Huang, H. Hou, X. Xie, C. Zhi, *Angew. Chem. Int. Ed. Engl.* **2017**, *56*, 9141.
[68] L. A. P. Kane-Maguire, G. G. Wallace, *Synth. Met.* **2001**, *119*, 39.
[69] C. F. Hsu, L. Zhang, H. Peng, J. Travas-Sejdic, P. A. Kilmartin, *Synth. Met.* **2008**, *158*, 946.
[70] S. Li, A. Liu, Z. Yang, J. He, J. Wang, F. Liu, H. Lu, X. Yan, P. Sun, X. Liang, Y. Gao, G. Lu, *Sens. Actuators B Chem.* **2019**, *299*.

